Differential cross sections of fine-structure transitions in K(4P)-He and -Ar collisions

J. M. Mestdagh, P. de Pujo, J. Pascale, J. Cuvellier, and J. Berlande
Service de Physique des Atomes et des Surfaces, Centre d'Etudes Nucleaires de Saclay, 91191 Gif-Sur-Yvette Cedex, France
(Received 11 July 1986)

Differential cross sections for the transition $K(4P_{3/2} \rightarrow 4P_{1/2})$ induced by He and Ar have been studied both experimentally and theoretically. Calculations were performed using a full quantal close-coupling formalism. The angular distribution of the scattered atoms is measured by Doppler shift (ADDS method). The comparison with the theoretical calculations is performed on the basis of thorough kinematic analysis. In addition, the polarization effects corresponding to the experimental conditions are taken into account carefully. This allows one to test the accuracy of various interaction potentials available for the K-He and -Ar systems. The most interesting result concerns the K-He l-dependent pseudopotentials, which are found accurate to a sufficiently high level to allow good predictions of the observed differential cross-section patterns. In particular the positions and amplitudes of the cross-section oscillations at large center-of-mass scattering angles are well reproduced. The results for Ar show that the K-Ar potentials must be improved. Finally, taking the K(4P)-He fine-structure transition as an example, it has been shown how polarization effects may be used in ADDS measurements to obtain information on the dynamics of the collision process.

I. INTRODUCTION

Fine-structure transitions (FST) in the first ^2P level of alkali-metal atoms (A) induced by low-energy collisions with ground-state rare-gas atoms (G) according to the reaction

$$A(^2P_j)+G \rightarrow A(^2P_{j' \neq j})+G \ , \tag{1}$$

where $j=\frac{1}{2}$ or $\frac{3}{2}$ may be considered as representative of more general inelastic collisions where electronic excitation is present in both the entrance and exit channels.

Early theoretical studies of process (1), as reviewed in Ref. 1, are based on semiclassical methods. They have clearly identified the main mechanisms responsible for FST. A close-coupling (CC) formalism which provides full quantal calculations of FST cross sections was developed by Reid[2] and Mies.[3] Presently, the knowledge of the alkali-metal—rare-gas interaction potentials appears to be the only factor which limits the accuracy of CC quantal calculations. Indeed, it is worthwhile to say that calculating interaction potentials goes necessarily through more or less approximate methods. A simple way for testing the validity of these methods is to compare experimental data for process (1) to CC calculations in as much detail as possible: thus FST appear as test processes for evaluating the accuracy of alkali-metal—rare-gas potential calculations. This has been exemplified in several studies of total cross sections for process (1), as, for example, in Ref. 4. However, it is well known that differential cross sections are much more sensitive to potential details than total cross sections. Therefore we report in this article on crossed-beam measurements and CC calculations concerning differential cross sections in order to go into more detailed comparisons between experiment and theory for process (1). The two following reactions have been considered:

$$K(4\,^2P_{3/2})+He \rightarrow K(4\,^2P_{1/2})+He \tag{2}$$

and

$$K(4\,^2P_{3/2})+Ar \rightarrow K(4\,^2P_{1/2})+Ar \ . \tag{3}$$

The study of process (2) is particularly interesting since l-dependent pseudopotentials have been made available recently for all the alkali-He pairs[5] and have been shown to reproduce accurately various available experimental data[6] (mainly line shape, far wing emission, and total cross sections for FST processes). It is therefore interesting to know if these potentials, in the case of K(4P)-He are realistic enough to accurately predict differential cross sections.

In a recent work comparisons have been made between CC calculations and experimental data concerning the energy dependence of total cross sections for process (3).[4] Various sets of adiabatic interaction potential curves were tested. They are those of Chebanier de Guerra and Masnou-Seeuw (denoted CM),[7] those of Duren *et al.*[8] (denoted DHM), and those of Pascale and Vandeplanque[9] (denoted PV). These potential sets are shown in Ref. 4. Two sets are found fairly realistic for interpreting FST total cross sections: the PV set over the range of K-Ar internuclear distances $R > 8$ a.u., and the CM set for $R < 15$ a.u. The CC calculations presented here for the differential cross section of process (3) use these three sets of potentials in order to test their accuracy.

When excited states of atoms are involved in crossed-beam studies of collisional processes, effects related to the polarization of the excited state often play an important role.[10–12] This has been illustrated in several studies of total cross sections for processes (2) and (3).[4,10,12] Obviously, these effects (called polarization effects) must be considered also when studying differential cross sections.

They have been included in the theoretical treatment of the present work to allow a direct comparison with the experimental results. As we shall see later on, this has made necessary the calculation of differential cross sections for the following elementary processes:

$$K(4\,^2P_j,m_j)+He\rightarrow K(4\,^2P_{j'},m_{j'})+He \tag{4}$$

and

$$K(4\,^2P_j,m_j)+Ar\rightarrow K(4\,^2P_{j'},m_{j'})+Ar\ . \tag{5}$$

The conventional way to measure differential cross sections is to link a crossed-beam apparatus to a rotating detector. It is not easy to apply here. An alternative method, the so-called ADDS method (angular distribution using the Doppler shift), has been used here. The method, originally introduced by Kinsey and co-workers[13–15] is based on the analysis of a Doppler absorption profile and has been applied recently for process (3).[16]

Previous studies of polarization effects in conventional (as compared to ADDS) differential cross-section measurements have allowed one to gain information on the collision dynamics.[11] The second aim of the present work is to show what information on the collision dynamics may be obtained from a study of polarization effects in ADDS differential cross-section measurements. This is done from a theoretical point of view taking process (2) as an example.

The experimental apparatus and the experimental method are described in Sec. II. The way to take the polarization effects into account under our experimental conditions is explained in Sec. III. The quantum-mechanical CC calculation method is outlined shortly in Sec. IV. The theoretical results are displayed in Sec. V. The experimental results are presented and compared to the theoretical predictions in Sec. VI. Finally, the general discussion of polarization effects in ADDS measurements is presented in Sec. VII.

II. EXPERIMENT

A. Principle

In conventional measurements of differential cross sections, the angular distribution of the scattered atoms is recorded using a crossed-beam apparatus and a detector which rotates in the plane of the two-particle beams. This method is inappropriate for studying FST processes because the inelastic process under study is mixed with elastic scattering. For example, process (2) is mixed with the process

$$K(4\,^2P_{3/2})+He\rightarrow K(4\,^2P_{3/2})+He\ . \tag{6}$$

The ADDS technique proposed by Kinsey and co-workers[13–15] has been used here to measure the inelastic processes (2) and (3) unmixed with the competing elastic processes. The efficiency of the method for studying FST processes has been proved already.[14,16] Let us recall briefly the technique.

The collisions between the K atoms and the rare-gas perturbers are realized in a crossed-beam geometry. The

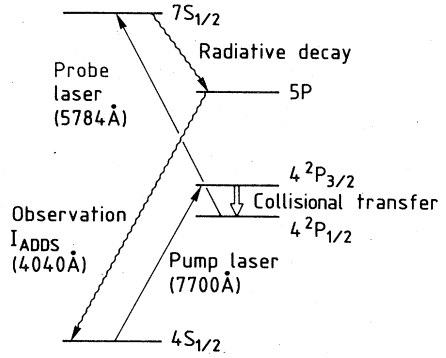

FIG. 1. Energy levels of K showing the excitation schemes of the lasers (pump laser and probe laser) and the detected fluorescence.

relative velocity $\mathbf{V}_r$ of the colliding partners is well defined both in magnitude and direction. A laser induced fluorescence technique is used to detect the K atoms scattered in the $4\,^2P_{1/2}$ level following the excitation scheme of Fig. 1. As shown in the Newton diagram of Fig. 2, the probe laser is set along the relative velocity vector, in the direction of the crossing zone of the two-particle beams. Because of the Doppler shift, the $K(4\,^2P_{1/2})$ atoms scattered under the angle θ with respect to $\mathbf{V}_r$ detect the laser photons at the frequency ν'

$$\nu'=\nu[1-V'_K\cos(\theta)/c-\mathbf{V}_{c.m.}\cdot\hat{\mathbf{n}}/c]\ ,$$

where ν is the laser frequency in the laboratory, $\mathbf{V}'_K$ is the center-of-mass velocity of the scattered K atoms, $\mathbf{V}_{c.m.}$ is the center-of-mass velocity in the laboratory, c is the velocity of light and $\hat{\mathbf{n}}$ is the unit vector in the probe laser direction. The excitation from $4\,^2P_{1/2}$ to $7\,^2S_{1/2}$ is achieved when the frequency ν' matches the resonance frequency ν_0 corresponding to the $4\,^2P_{1/2}$–$7\,^2S_{1/2}$ splitting. The excitation condition can be written

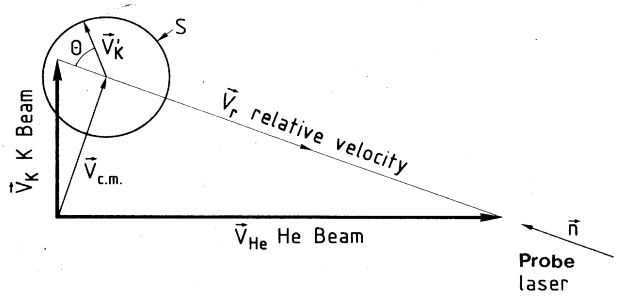

FIG. 2. Newton Diagram for process (2). The laboratory velocities of He and K are $\mathbf{V}_{He}$ and $\mathbf{V}_K$. The relative velocity and the center-of-mass velocities are $\mathbf{V}_r$ and $\mathbf{V}_{c.m.}$. The velocity of the atoms scattered under the center-of-mass angle is V'_K. $\mathbf{V}'_K$ is distributed on the sphere S. The probe laser is directed along $\hat{\mathbf{n}}$.

TABLE I. Characteristics of the particle beams: average velocity of the atoms ($\overline{V}$), Mach number (M), full width at half maximum of the velocity distribution (ΔV), and angular divergence of the beam.

Beam	$\overline{V}$ (m/s)	M	ΔV (m/s)	Angular divergence
He	2700	24	200	1°
Ar	640	27	40	1°
K	938	7	340	0.5°

TABLE II. Characteristics of the lasers.

	Pump laser	Analysis laser
Laser direction	Perpendicular to the particle beam plane	Along the relative velocity vector
Polarization	Circular	Circular
Frequency width	1 MHz	1 MHz

$$\frac{\nu-\nu_0}{\nu_0}\approx\frac{\nu-\nu_0}{\nu}=V'_K\cos(\theta)/c+\mathbf{V}_{c.m.}\cdot\hat{\mathbf{n}}/c\ . \tag{7}$$

The intensity I_{ADDS} of the fluorescence emitted by the $7S_{1/2}$ level is proportional to the number of atoms which are excited when the probe laser is tuned to the frequency ν. This number is itself proportional to the amount of atoms scattered in the direction θ, θ, and ν being related by Eq. (7). More exactly, since the frequency width of the probe laser is constant as ν is tuned, the intensity $I_{ADDS}(\nu)$ is proportional to the differential cross section per solid angle in the center-of-mass reference frame:

$$I_{ADDS}(\nu)\sim\frac{d\sigma}{d\Omega}\ . \tag{8}$$

Therefore the differential cross-section measurement is achieved by recording I_{ADDS} as a function of the laser frequency ν. It is important to notice that the ADDS method has a cylindrical symmetry with respect to the direction of $\mathbf{V}_r$ since the K atoms are detected whatever their azimuthal angle around $\mathbf{V}_r$ is.

B. Apparatus

The experimental apparatus used here has been described elsewhere in most aspects.[17] The potassium and rare-gas beams are crossed at right angle. Their characteristics are reported in Table I. The pump laser is tuned to the transition $4\,^2S_{1/2}\ F=2\rightarrow 4\,^2P_{3/2}\ F=3$ to populate the K atom in the appropriate excited level. The Doppler absorption profile of the transition $4\,^2P_{1/2}\rightarrow 7\,^2S_{1/2}$ is scanned by the probe laser. The excitation scheme is shown in Fig. 1. The characteristics of the two lasers are given in Table II. A photon counting system allows one to measure the fluorescence intensity I_{ADDS} emitted by the $7S$ level of K over the transition $5P\rightarrow 4S$ (the level $5P$ is populated from $7S$ by radiative decay). The detection scheme is also shown in Fig. 1. Finally, the intensity I_{ADDS} is recorded as a function of the probe laser frequency using a multi-channel analyzer (MCA). A sweep is used for both scanning the laser frequency and for triggering the MCA.

C. Angular resolution

The tuning condition (7) allows a first estimation of the angular resolution given by the ADDS method. Because of the cosine term in (7), the resolution is maximum when the center-of-mass scattering angle is about 90°.

The most important point, however, concerns the effect of the particle-beam characteristics on the resolution. The particle beams have indeed a finite collimation ratio and a finite velocity width. Therefore the vectors $\mathbf{V}_K$, $\mathbf{V}_{He}$, and $\mathbf{V}_r$ of Fig. 2 are mean velocity vectors. The corresponding actual velocity vectors are noted $\mathscr{V}_K$, $\mathscr{V}_{He}$, and $\mathscr{V}_r$. As a result, the collisional situation schematized in Fig. 2 is an average of elementary situations in which the probe laser direction $\hat{\mathbf{n}}$ is not necessarily parallel to $\mathscr{V}_r$. This is the important point which affects the angular resolution of the method. Let the ADDS signal corresponding to each of these elementary situations be $\mathscr{I}(\mathscr{V}_{He},\mathscr{V}_K,\nu')$ where ν' is the frequency of the probe laser. Then, the measured signal I_{ADDS} is given by the following average:

$$I_{ADDS}(\nu)=\int\int\int\Phi_{He}(\mathscr{V}_{He})\Phi_K(\mathscr{V}_K)\Phi_{laser}(\nu'-\nu)\mathscr{I}(\mathscr{V}_{He},\mathscr{V}_K,\nu')d\mathscr{V}_{He}d\mathscr{V}_K d\nu'\ . \tag{9}$$

In Eq. (9) the integrations are performed over the He and K velocity distributions $\Phi_{He}(\mathscr{V}_{He})$ and $\Phi_K(\mathscr{V}_K)$. Now, the probe laser operates under single-mode conditions, but very small secondary modes are also present with intensities which are less than 1% of the principal mode. Therefore, in order to account for them, average has also been made in Eq. (9) over the probe laser frequency. Let us notice here that no average over the interaction time between the scattered atoms and the probe laser appears in Eq. (9). This interaction time is indeed entirely determined by the lifetime of the $4P_{1/2}$ of about 30 ns.

The quantity $\mathscr{I}(\mathscr{V}_{He},\mathscr{V}_K,\nu')$ in Eq. (9) is given by

$$\mathscr{I}(\mathscr{V}_{He},\mathscr{V}_K,\nu')=A\tau\sum_{i=1,2}\int d\varphi\sin(\theta_i)\left[\frac{d\sigma}{d\Omega}\right]_{\theta=\theta_i}\left[\frac{d\theta}{d\nu'}\right]_{\theta=\theta_i}\frac{n_{He}n_K}{\mathscr{V}_{He}\mathscr{V}_K}\mathscr{V}_r\ , \tag{10}$$

where n_{He} and n_K are, respectively, the flux of He and K in the atomic beams; τ is the volume of the scattering zone and A a proportionality factor which includes the efficiency of the photon counting system and the oscillator strength of the transitions $4P_{1/2} \rightarrow 7S_{1/2}$, $7S_{1/2} \rightarrow 5P$, and $5P \rightarrow 4S$ involved in the detection procedure. Since, in general, $\hat{\mathbf{n}}$ is not parallel to $\mathscr{V}_r$, elementary ADDS situations do not have cylindrical symmetry with respect to $\mathscr{V}_r$. Therefore, the velocity in the center-of-mass reference frame $\mathscr{V}'_K$, of the scattered K atoms must be characterized by two polar angles: The angle between $\mathscr{V}'_K$ and $\mathscr{V}_r$ and the azimuthal angle φ around $\mathscr{V}_r$. These two angles are related by the tuning condition

$$\frac{\nu'-\nu_0}{\nu_0} \approx \frac{\nu'-\nu_0}{\nu'} = (\mathscr{V}'_K \cdot \hat{\mathbf{n}} + \mathscr{V}_{\text{c.m.}} \cdot \hat{\mathbf{n}})/c \ , \tag{11}$$

where $\mathscr{V}_{\text{c.m.}}$ is the center-of-mass velocity. Considering θ as a function of ν' and φ, Eq. (11) has, in general, two solution, θ_1 and θ_2. These solutions are those used in Eq. (10) to calculate $\mathscr{I}(\mathscr{V}_{He}, \mathscr{V}_K, \nu')$ explicitly. It is interesting to notice that Eqs. (11) and (10) reduce to Eqs. (7) and (8) for the Newton diagram of Fig. 2.

Finally, it is important to mention that the comparisons between theory and experiment are done after numerical averaging of the theoretical data calculated in Sec. V using Eqs. (9)—(11) and the beam characteristics listed in Table I.

III. POLARIZATION EFFECTS UNDER OUR EXPERIMENTAL CONDITIONS

A. Effects linked to the excitation scheme of the probe laser

Derivation of Eq. (8) assumes an isotropic distribution of the electronic angular momentum in the excited $4P_{1/2}$ level. Generally speaking, the detection of this level by laser-induced fluorescence may depend on the state of polarization of this level which may vary itself with the scattering angle. Thus a careful choice of the detection scheme must be made to remove these difficulties. In this connection, the excitation scheme shown in Fig. 1 and Table II is appropriate since in this case, the ADDS signal actually does not depend on the state of polarization of the scattered atoms. This can be shown explicitly using the formalism of irreducible components of density matrixes.[18] The demonstration is cumbersome but straightforward. The key point in this demonstration is that the hyperfine (hf) structure of K can be ignored. To prove it the following points must be considered. (i) The detection of the fluorescence coming from the $7S_{1/2}$ level is not sensitive either to the hf structure of this level nor to its polarization state. (ii) The width of the probe laser is much larger than the hf structure of the $7S_{1/2}$ level. (iii) The Doppler width of the $4P_{1/2} \rightarrow 7S_{1/2}$ transition is much larger than the hf structure of the $4P_{1/2}$ level. As a result, the K atoms which are scattered in the level $4P_{1/2}$ with the direction θ and the wave vector $\mathbf{k}_{1/2}$ (in the center-of-mass reference frame) are entirely described by four irreducible density matrix components; namely, ${}_{4^2P_{1/2}}\rho_0^0(\mathbf{k}_{1/2})$ (population of the $4^2P_{1/2}$ level) and ${}_{4^2P_{1/2}}\rho_q^1(\mathbf{k}_{1/2})$ with $q=-1$, 0, or $+1$. These matrix components are, respectively, the tensorial orders 0 (population) and 1 (orientation) of the density matrix describing the $4^2P_{1/2}$ level. The other important point of the demonstration is that the probe laser is linearly polarized. Then only even tensorial order of the $4^2P_{1/2}$ level density matrix can be detected by laser-induced fluorescence. As a result, the ADDS signal I_{ADDS} is proportional to the $k=0$ tensorial orders of the $4^2P_{1/2}$ level density matrix, i.e.,

$$I_{\text{ADDS}}(\nu) \sim {}_{4^2P_{1/2}}\rho_0^0(\mathbf{k}_{1/2}) \ . \tag{12}$$

B. Effects linked to the excitation scheme of the pump laser

Because a laser is used to populate the K atoms in the $4^2P_{3/2}$ level before collision, polarization is induced in these atoms. As a result, the differential cross section expressed by $d\sigma/d\Omega$ in Eqs. (8) and (10) is not the conventional differential cross section of processes (2) or (3) where equal population is assumed in the magnetic sublevels of the $4^2P_{3/2}$ and $4^2P_{1/2}$ levels. It is in fact a combination of the scattering amplitudes of the elementary processes (4) and (5) which must be determined. This is done by relating the density matrix ${}_{4^2P_{1/2}}\rho(\mathbf{k}_{1/2})$ describing the atoms after the collision to the density matrix ${}_{4^2P_{3/2}}\rho(\mathbf{k}_{3/2})$ describing the K atoms before the collision. Here the vectors $\mathbf{k}_{3/2}$ and $\mathbf{k}_{1/2}$ are the wave vectors of the K atoms before and after collision, respectively. The formalism used to derive this relation is very close to that used in our previous work.[10] It uses a space-fixed reference frame, in which the z axis is along the initial relative velocity vector (i.e., along $\mathbf{k}_{3/2}$). Defining by $\Gamma(4^2P_{3/2}\ \mathbf{k}_{3/2} \rightarrow 4^2P_{1/2}\ \mathbf{k}_{1/2})$ (more simply written Γ) the collision matrix describing the collisional process (see Appendix), the relation appears as to be

$${}_{4^2P_{1/2}}\rho(\mathbf{k}_{1/2}) = \frac{1}{\sigma}\Gamma\ {}_{4^2P_{3/2}}\rho(\mathbf{k}_{3/2})\Gamma^\dagger \ , \tag{13}$$

where $\Gamma^\dagger$ is the adjoint operator of Γ, and where the total cross section σ of the collisional process has been introduced for normalization purposes.

Equation (13) can be simplified by keeping in mind that the ADDS method has an average cylindrical symmetry (see Sec. II). It is convenient for that to expand Eq. (13) on the following irreducible tensorial set:[18]

$${}^JT_q^{(k)} = \sum_{M,N} (-1)^{J-N} \langle J\,J\,M\,-N \mid k\,q \rangle \mid JM \rangle \langle JN \mid \ .$$

After expansion on this tensorial set, Eq. (13) allows one to calculate the population transferred in the $4^2P_{1/2}$ by the collision. It is given by

$${}_{4^2P_{1/2}}\rho_0^0(\mathbf{k}_{1/2}) = \frac{1}{\sigma}\sum_{k,q} \Gamma_{0q}^{0k}\ {}_{4^2P_{3/2}}\rho_q^k(\mathbf{k}_{3/2}) \ . \tag{14}$$

In Eq. (14) ${}_{4\,^2P_{3/2}}\rho_q^k(\mathbf{k}_{3/2})$ are the irreducible components of the density matrix ${}_{4\,^2P_{3/2}}\rho(\mathbf{k}_{3/2})$, and $\Gamma_{q'q}^{k'k}$ are those of the collision matrix Γ. Notice that only the components Γ_{0q}^{0k} appear in Eq. (14).

The ADDS measurement technique ensures cylindrical symmetry with respect to $\mathbf{V}_r$. Since the quantization axis z is along $\mathbf{V}_r$, the following selection rules result from Eq. (A4) of the Appendix:

$$\Gamma_{0q}^{0k}=\delta_{q0}\Gamma_{00}^{0k},\quad k \text{ even}. \tag{15}$$

Inserting Eq. (15) into Eq. (14) and using Eq. (12), the following expression is obtained for the ADDS signal:

$$I_{\mathrm{ADDS}}(v)\sim\Gamma_{00}^{00}{}_{4\,^2P_{3/2}}\rho_0^0(\mathbf{k}_{3/2}) + \Gamma_{00}^{02}{}_{4\,^2P_{3/2}}\rho_0^2(\mathbf{k}_{3/2})\ . \tag{16}$$

Equation (16) is general provided that the density matrix and the collision matrix are referred to a space-fixed reference frame with z axis set along the initial relative velocity vector of the colliding partners.

Equation (16) is the same as that found in Ref. 10 when considering total cross sections. The reason is that the selection rules (15) express a common cylindrical symmetry for both total cross section and ADDS differential cross-section measurements.

The population and longitudinal alignment of the $4P_{3/2}$ level corresponding to the excitation scheme of Table II are deduced from Ref. 10. They are given by

$${}_{4\,^2P_{3/2}}\rho_0^0(\mathbf{k}_{3/2})=\tfrac{1}{2};\quad {}_{4\,^2P_{3/2}}\rho_0^2(\mathbf{k}_{3/2})=-\tfrac{1}{4}\ . \tag{17}$$

Using Eqs. (17) and (A1), Eq. (14) becomes

$$I_{\mathrm{ADDS}}(v)\propto\frac{d\sigma}{d\Omega}=\frac{1}{4}\left[\left[\frac{d\sigma}{d\Omega}\right]_{3/2}+3\left[\frac{d\sigma}{d\Omega}\right]_{1/2}\right], \tag{18}$$

with

$$\left[\frac{d\sigma}{d\Omega}\right]_{3/2}=\frac{d\sigma(P_{3/2+3/2}\rightarrow P_{1/2+1/2})}{d\Omega}+\frac{d\sigma(P_{3/2+3/2}\rightarrow P_{1/2-1/2})}{d\Omega} \tag{18'}$$

and

$$\left[\frac{d\sigma}{d\Omega}\right]_{1/2}=\frac{d\sigma(P_{3/2+1/2}\rightarrow P_{1/2+1/2})}{d\Omega}+\frac{d\sigma(P_{3/2+1/2}\rightarrow P_{1/2-1/2})}{d\Omega}\ , \tag{18''}$$

where the $[d\sigma(P_{3/2\,m}\rightarrow P_{1/2\,m'})/d\Omega]$'s are the cross sections of the elementary processes (4) and (5). Equation (18) relates the ADDS signal to the cross sections of the elementary processes (4) or (5).

IV. QUANTUM-MECHANICAL CLOSE-COUPLING CALCULATION

The quantum-mechanical formulation of the scattering theory describing the collision of an alkali atom excited in a $n\,^2P_{jmj}$ state with a structureless ground-state rare-gas atom is well known.[2,3] The present close-coupling calculation uses the space-fixed formulation described by Reid.[2] The main inputs in this method are two quantities $\hat{v}_0(R)$ and $\hat{v}_2(R)$ which allow one to calculate the matrix elements of the close-coupling equations. It is important to recall that these quantities define an effective interaction which reproduces exactly the known adiabatic potential energy curves $V_{A\,^2\Pi}$ and $V_{B\,^2\Sigma}$ relevant to the $n\,^2P$ level. They are defined by

$$\hat{v}_0(R)=\tfrac{1}{3}[V_{B\,^2\Sigma}(R)+V_{A\,^2\Pi}(R)]\ ,$$
$$\hat{v}_2(R)=\tfrac{5}{3}[V_{B\,^2\Sigma}(R)-v_{A\,^2\Pi}(R)]\ .$$

The integration of the close-coupling equations allows one to determine the T matrix from which the differential cross sections can be derived. The details of the calculations and notations can be found in our previous work.[12] The space-fixed reference frame is chosen to have a z axis set along the incident relative wave vector $\mathbf{k}_j$. It can be shown that the differential cross section for collisionally induced transition between the magnetic sublevels of the excited alkali-metal atom reduces to the expression

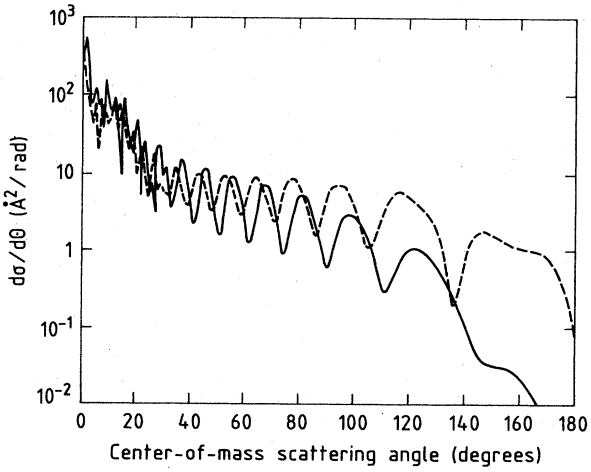

FIG. 3. Differential cross section for the $4\,^2P_{3/2}\rightarrow 4\,^2P_{1/2}$ transition in K $(4\,^2P)$ + He collisions at 0.15 eV with the entrance channels $B\,^2\Sigma_{1/2}$ (dashed curve) and $A\,^2\Pi_{3/2}$ (solid curve). See text. Quantum-mechanical calculations using the potentials of Ref. 5.

$$\frac{d\sigma}{d\hat{\mathbf{R}}}(jm_j \to j'm_{j'};\hat{\mathbf{R}}) = \frac{\pi}{k_j}\sum_{1,1'} |\, i^{1+1'}(2l+1)\mathscr{G}_{1\,1'\,m_j} Y_{l'\,m_j-m_{j'}}(\hat{\mathbf{R}})\,|^2 , \tag{19}$$

where

$$\mathscr{G}_{1\,1'\,m_j} = \sum_J \langle j\,1\,m_j\,0\,|\,J\,m_j\rangle T^J(j'\,l';j\,l)\langle j'\,l'\,m_{j'}\,m_j - m_{j'}\,|\,J\,m_j\rangle .$$

The conventional differential cross section for the FST processes is calculated as

$$\frac{d\sigma}{d\Omega}(j \to j';\hat{\mathbf{R}}) = \frac{1}{2j+1}\sum_{m_j,m_{j'}} \frac{d\sigma}{d\hat{\mathbf{R}}}(jm_j \to j'm_{j'};\hat{R}) . \tag{20}$$

Equation (19) allows one to evaluate the differential cross section to be effectively compared with the experimental one, that is, taking into account the polarization effects under the experimental conditions [see Eq. (18)].

V. THEORETICAL RESULTS

A. Results for K-He

The differential cross sections of the elementary process (4) have been calculated using the potential set of Ref. 5 for various energies ranging between 0.15 and 0.17 eV. When included in Eqs. (18′) and (18″) the quantities $(d\sigma/d\theta)_{3/2}$ and $(d\sigma/d\theta)_{1/2}$ are obtained. They represent the differential cross section of process (2) when the K-He system enters the collision respectively on the potential curves $A\,^2\Pi_{3/2}$ or $B\,^2\Sigma_{1/2}$. They are shown in Fig. 3 for one typical collision energy of 0.15 eV. The cross section which includes the polarization effects corresponding to the experimental conditions is deduced from Eq. (18). It is shown in Fig. 4 for the same collision energy.

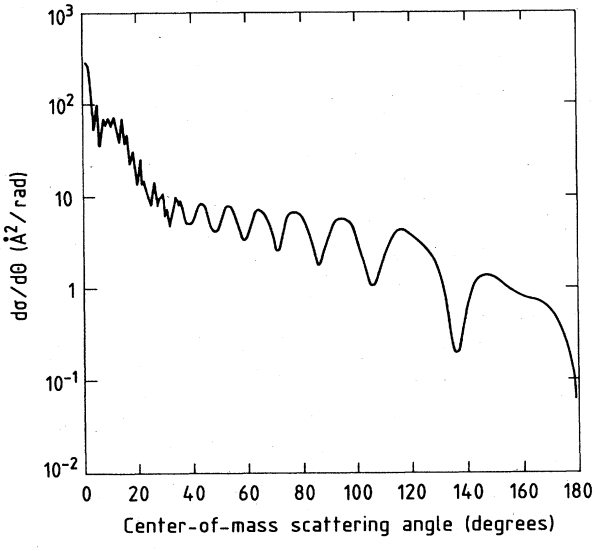

FIG. 4. Differential cross section for the $4\,^2P_{3/2} \to 4\,^2P_{1/2}$ transition in K $(4\,^2P)$ + He collisions at 0.15 eV. Quantum-mechanical calculations using the potentials of Ref. 5. The polarization effects given by Eq. (18) are included.

Several features are observed in Figs. 3 and 4.

(a) The cross section is peaked in the forward direction (center-of-mass scattering angle smaller than 30°). This is expected for inelastic processes such as process (2).

(b) In the region of forward scattering, the oscillatory structure of the cross section is complex. Saxon *et al.*[19] have discussed the origin of similar oscillations in Na(3*P*)-Ar FST. They are connected to rainbow scattering (rainbow, supernumerary rainbows, and superimposed rapid oscillations) in the well of the $A\,^2\Pi$ curve of the interaction potentials. The rainbow scattering of the K(4*P*)-He system is, however, more complex than that seen with Na(3*P*)-Ar. The fine-structure splitting of K(4*P*) (57 cm^{-1}) is only four times smaller than the well depth of the K-He $A\,^2\Pi$ potential curve (245 cm^{-1}). As a result the rainbow patterns for scattering on the $A\,^2\Pi_{3/2}$ and $A\,^2\Pi_{1/2}$ potential curves are slightly different. This leads to additional interference effects which are unknown in the Na-Ar collision. Such a behavior has already been encountered in other FST processes, and was considered as an indication that the electron spin remains coupled to an appreciable extent during the collision.[20]

(c) At larger center-of-mass scattering angles ($\theta > 40°$), the cross section has regular oscillations. They are attributed to interferences from scattering on the $A\,^2\Pi$ and $B\,^2\Sigma$ potentials.[21–23] A very simple formula based on classical mechanics considerations has been proposed to account for the number $N(\theta)$ of such oscillations per radian around a center-of-mass scattering angle θ.[22] It is

$$N(\theta)\,|\,b_\Sigma - b_\Pi\,|\,(2\mu E)^{1/2}/h , \tag{21}$$

where μ is the reduced mass of the colliding system, E is the collision energy, b_Σ is the impact parameter leading to the classical deflection θ for scattering on the $B\,^2\Sigma$ potential, and b_Π is the same quantity for scattering on the $A\,^2\Pi$ potential. Equation (21) is found accurate to within 10% for center-of-mass scattering angles ranging between 50° and 110°. This formula can be of some help for providing qualitative information on the interaction potentials when theoretical predictions of FST cross sections are compared to experimental results.[21]

Finally, it is observed in Fig. 3 that the features *a* to *c* mentioned above are qualitatively similar but qualitatively different for the two entrance channels $B\,^2\Sigma_{1/2}$ or $A\,^2\Pi_{3/2}$. (i) The oscillations of the cross section are shifted from one entrance channel to the other. (ii) The entrance on the $B\,^2\Sigma_{1/2}$ channel leads to larger values of the cross section at large scattering angle than the entrance on the other channel. (iii) The reverse is observed at small scattering angle. These differences stress on the fact that polarization effects are important when considering the differential cross section for process (2).

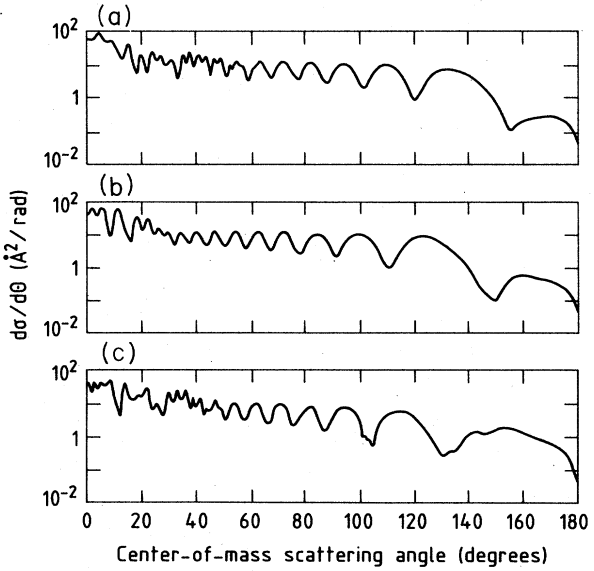

FIG. 5. Differential cross section for the $4\,^2P_{3/2} \rightarrow 4\,^2P_{1/2}$ transition in K $(4\,^2P)$ + Ar collisions at 0.13 eV. Quantum-mechanical calculations using the potential sets DHM (a), PV (b), and CM (c). The polarization effects given by Eq. (18) are included.

B. Results for K-Ar

The theoretical predictions for process (3) are reported in Fig. 5 for the three potential sets DHM, PV, and CM mentioned in the introduction. Polarization effects are included according to Eq. (18) and the collision energy is 0.13 eV. Qualitatively, these results are similar to those encountered with He: forward peaked cross section, rainbow oscillations in the forward scattering, and regular oscillation at larger scattering angles. However, the forward peaking is less pronounced in the case of Ar. It is interesting to notice that the extension of the region of rainbow scattering is smaller for the potential set PV than for the other potentials. This reflects the well depth of the $A\,^2\Pi$ potential which is about 250 cm^{-1} for the set PV against 450 cm^{-1} for the potentials DHM and CM. The phase of the regular oscillations at large scattering angle is different for the three sets of potentials. This illustrates that the region of backward scattering in the differential cross section is sensitive to the shape of the potential curves used in the CC calculations. This result is particularly important since the comparison between experiment and theory carried out in the following two sections mainly concerns the region of backward scattering.

VI. COMPARISON BETWEEN EXPERIMENT AND THEORY

A. The K-He system

The experimental results for process (2) are shown in Fig. 6 (points) for an average collision energy of 0.16 eV. They give the differential cross section as a function of the frequency offset of the probe laser. Note that the frequency scale is related to the center-of-mass scattering angle through Eq. (7). The corresponding angular scale is also given in the figure. The zero frequency offset corresponds to forward scattering ($\theta = 0°$).

The signal I_{ADDS} shown in Fig. 6 extends below $\theta = 0°$ and above $\theta = 180°$. This reflects that the velocity distributions of the particle beams have finite widths. As explained in Sec. II C, this point is taken into account in the comparison between experiment and theory by averaging the theoretical data of Sec. V over the beam characteristics reported in Table I. Note that the energy dependence of the differential cross section is taken into account in this average. The theoretical results are shown in Fig. 6 along with the experimental data. The main consequence of the averaging is to smear out the rapid oscillations in the forward scattering region (see Fig. 4 for comparison). For scattering angles larger than 60 degrees, the regular oscillations are resolved.

When comparing experimental and theoretical results in Fig. 6 several features may be observed. (1) The experimental results confirm that the cross section is forward peaked. The forward-backward scattering ratio is well predicted by theory. (2) The experiment confirms the existence of regular oscillations in the cross section at large scattering angle ($\theta > 60$ degrees). The amplitudes and positions of these oscillations are well predicted except for the very last oscillation (corresponding to extreme backward scattering) which is predicted in position only. This comparison is a stringent test of the accuracy of the potential curves used in the CC calculation, since as shown in Sec. V B, the differential FST cross sections are sensitive to the details of potential in the region of backward scattering.

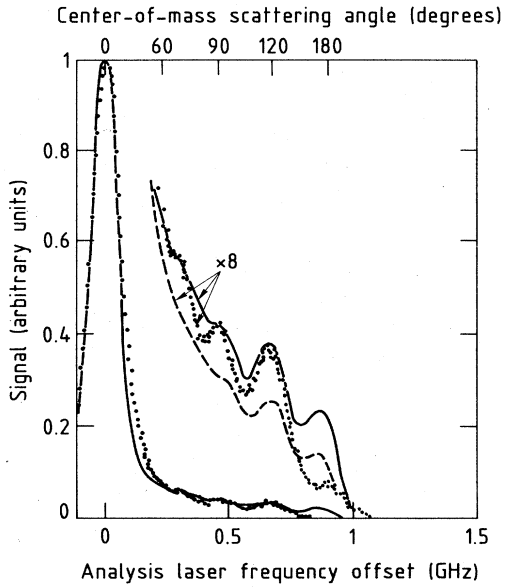

FIG. 6. Differential cross section for the $4\,^2P_{3/2} \rightarrow 4\,^2P_{1/2}$ transition in K $(4\,^2P)$ + He collisions at 0.16 eV: experimental results (dotted curve) and the corresponding theoretical prediction (solid curve). The dashed curve gives the conventional cross section.

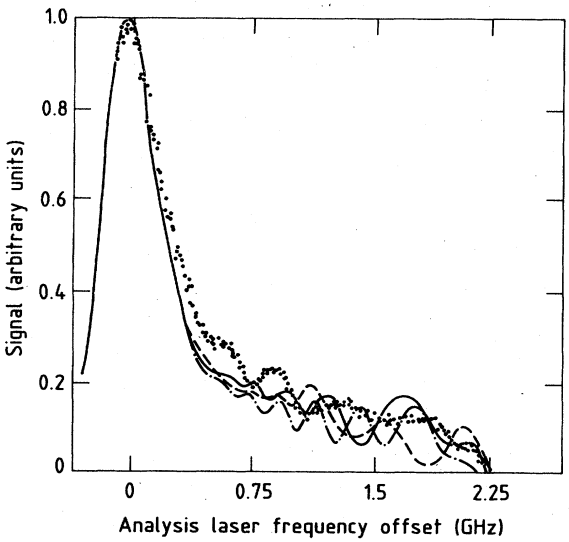

FIG. 7. Differential cross section for the $4^2P_{3/2} \rightarrow 4^2P_{1/2}$ transition in K (4^2P) + Ar collisions at 0.13 eV: experimental results (dotted curve) and the corresponding theoretical prediction done using the potential sets PV (solid curve), CM (dashed curve) and DHM (dotted-dashed curve).

(3) Polarization effects are included in the above calculation. For comparison, the dashed curve in Fig. 6 gives the conventional differential cross section of process (2) which does not take into account the polarization effects. Comparison of this curve with the experimental results shows markedly different oscillation patterns. This stresses a third important aspect of Fig. 6: the experimental data are compatible with the polarization effects predicted theoretically.

It is worth recalling two conclusions of a previous work[5] concerning the absolute value of the total cross section for process (2). Quantal CC calculations based on the same potential set as here were found in agreement with cross-beam measurements for (i) the absolute value of the cross section within a 15% uncertainty and (ii) the energy dependence of the cross section. For the full energy range experimentally investigated, i.e., from 0.02 to 0.35 eV, the agreement between experiment and theory was found within the experimental uncertainties (10—15%).

Points (i) and (ii) and (1)—(3) above attest of the accuracy of the *l*-dependent pseudopotentials calculated for the K ($4P$)-He system. Indeed, they allow one to interpret all the experimental data presently available on process (2). This process thus appears as a "reference" process where theoretical predictions are fairly safe. This possibility is used in Sec. VII following.

B. The K-Ar system

The differential cross section of process (3) measured experimentally is shown in Fig. 7 along with the theoretical results. The average collision energy is 0.13 eV. The polarization effects and the various averaging procedures according to the experimental conditions are included in the theoretical predictions.

The experimental results of Fig. 7 show that the cross section for process (3) is forward peaked and has regular oscillations in the backward scattering direction. This confirms qualitatively the theoretical predictions drawn in Sec. V B. The experimental results are in agreement with the previous experimental work of Duren *et al.*[16]

When comparing theoretical and experimental results in Fig. 7 for K-Ar, agreement is observed only for the overall shape of the cross section, but none of the potential sets leads to a good prediction of both the position and amplitude of the cross section oscillations as it was found for the K-He collision.

As outlined in Sec. V, the backward scattering oscillations of the cross section are due to interferences from scattering on the $A\,^2\Pi$ and $B\,^2\Sigma$ potential curves. The disagreement seen in Fig. 7 reflects inaccuracies in the three potential sets used in the calculation. We can exclude inaccuracies due to the treatment of the collision dynamics since it is done quantum mechanically by CC calculations.

From a previous work[4] concerning the total cross section of process (3), we know that the $B\,^2\Sigma$ curve of the potential set DHM presents an unreal well of about 80 cm^{-1} depth at a K-Ar distance of 12 a.u. This induces additional nonadiabatic coupling during the collision, and probably affects the scattering on the $B\,^2\Sigma$ potential curve. Inaccuracies may result in the predictions of the regular backward oscillations of the cross section. Corrections to the $B\,^2\Sigma$ curve of the DHM potential set have been suggested by Düren and co-workers.[16] They have initiated work in this direction.[23] On the contrary the $A\,^2\Pi$ potential curve of the set DHM may be considered as accurate since it has been optimized to agree with conventional differential scattering experiments.[16] The set PV was found realistic enough to interpret correctly the total cross section of process (3). However, it was pointed out that these potential curves are tested for K-Ar distances larger than 8 a.u. The range of internuclear distances involved in the backward scattering region of the differential cross section extends to shorter K-Ar separations. The comparison between experiment and theory in Fig. 7 thus suggests inaccuracies of the PV potential set in this region.

The observation of Fig. 7 shows that the potential set CM leads to a more rapidly oscillating differential cross section than found experimentally. Such a result seems surprising since the potential set CM is believed to be realistic over a wide range of K-Ar distances. The $A\,^2\Pi$ curve in the well region is close to the corresponding curve of the potential set DHM which has been fitted to interpret experimental data.[13] Moreover, the overall shape of the potential set CM is accurate enough to interpret total cross-section measurements.[4] The results of Fig. 7 thus indicate that these potentials are not yet accurate enough to give reliable predictions of differential cross-section patterns. Since backward scattering is involved, this probably concerns the repulsive part of the potentials. These conclusions apply as well to the two other potential sets PV and DHM.

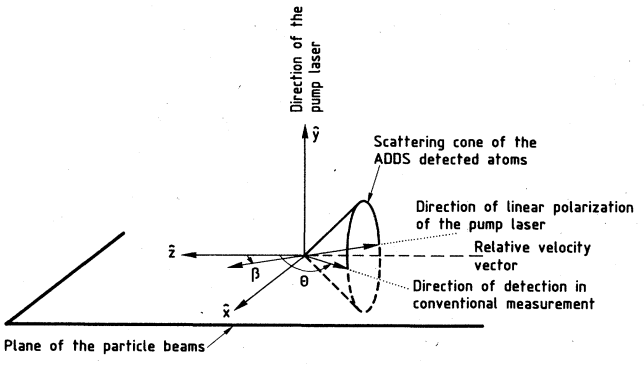

FIG. 8. Excitation and detection scheme allowing polarization effect studies in ADDS and conventional differential cross-section measurements.

VII. GENERAL FORMULATION OF POLARIZATION EFFECTS IN ADDS MEASUREMENTS

From Sec. V we know that polarization effects may be important in ADDS measurements. An interesting idea is to see what kind of information can be gained on the collisional dynamics when analyzing systematically these effects. Polarization effects have received much attention with this goal in mind when differential cross sections are measured using the conventional technique and when electronic excitation is present in the collision partners before the collision. Reference 11 gives a general review of the topic. We use this work as a guideline for the present discussion of polarization effects in ADDS measurements. The discussion is done from a theoretical point of view, taking process (2) as an example. This process was proposed as a reference process above in Sec. VI A. However, most of the conclusions drawn here are easy to extend to a variety of inelastic processes where the initial state of the atomic collision partner is electronically excited.

To compare ADDS measurements to conventional differential cross-section measurements, the best procedure is to write down an expression relating the detected signal I_D to the density matrix which describes the polarization of the excited atoms in the entrance channel. We make the assumption (valid for both ADDS and conventional measurements) that I_D is proportional to the population of atoms transferred by the collision into the final level [$4P_{1/2}$ level for process (2) in ADDS measurements]. This expression can be obtained, for example by including Eq. (12) into (10):

$$I_D \propto \sum_{k \text{ even}} \Gamma^{0k}_{00}\rho^k_0 + \sum_{k,q>0} 2\,\mathrm{Re}(\Gamma^{0k}_{0q}\rho^k_q)\,, \tag{22}$$

where Re ( ) means "real part of ( )", the terms ρ^k_q are the irreducible components of the density matrix describing the quantum state of the atoms before the collision (entrance channel), and the terms $\Gamma^{k'k}_{q'q}$ are the irreducible components of the collision matrix which describes the collisional process under study as defined in Sec. III B.

Equation (22) is quite general. In particular, it contains no assumption concerning the symmetry properties of the detection technique. As a result Eq. (22) contains all possible polarization effects in ADDS or conventional measurements. These correspond to the various values of the terms ρ^k_q that one can create when varying the pump laser excitation scheme.

Equation (22) is separated into two parts: (i) the summation $\sum_{k \text{ even}}$ which contributes to the signal in both measurement techniques and (ii) the second summation which contributes to the signal in conventional measurements only [in ADDS measurements this term disappears, due to axial symmetry; see the selection rule (15)]. With regard to Eq. (22), it is clear that the main difference between the two measurement techniques is due to symmetry considerations. The consequences of this point are easier to evaluate by considering the following example. The K atoms are prepared in the $4P_{3/2}$ level by the excitation $4S_{1/2} \rightarrow 4P_{3/2}$ using the excitation scheme of Fig. 8. The terms ρ^k_q describing the $4P_{3/2}$ level are then given by

$$\rho^0_0 = \tfrac{1}{2},\ \rho^1_q = 0,\ \rho^2_0 = -\tfrac{1}{4}(3\cos^2\beta - 1)\,,$$
$$\rho^2_{+1} = (\tfrac{3}{8})^{1/2}\sin\beta\cos\beta\,,\ \rho^2_{+2} = -(\tfrac{3}{32})^{1/2}\sin^2\beta\,, \tag{23}$$

Eq. (22) becomes

$$I_D \propto \tfrac{1}{2}\Gamma^{00}_{00} - \tfrac{1}{4}(3\cos^2\beta - 1)\Gamma^{02}_{00} + [(\tfrac{3}{2})^{1/2}\sin\beta\cos\beta\ \Gamma^{02}_{01} - (\tfrac{3}{8})^{1/2}\sin^2\beta\ \Gamma^{02}_{02}]\,. \tag{24}$$

The excitation scheme of Fig. 8 is common in differential cross-section measurements done with the conventional technique. The idea is to set the detector at a scattering angle θ and to record the variation of I_D as β is varied. Eq. (24) tells one what observations can be expected: an

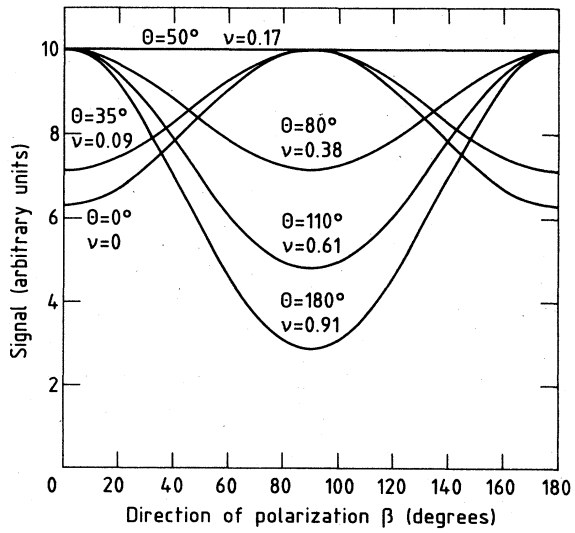

FIG. 9. Predicted effects in ADDS measurements for process (2) when the experimental arrangements of Fig. 8 is used.

oscillatory variation of I_D where the extrema do not correspond exactly to $\beta=0$ or $\beta=90$ degrees because of the term $\sin\beta\cos\beta$. This phenomenon has been observed, for example, in the inelastic process

$$\mathrm{Na}(3P)+\mathrm{Na}^+\rightarrow\mathrm{Na}(3S)+\mathrm{Na}^+$$

and has given information on the collision dynamics (in our formalism, this means that the experimental data provide information on the collision matrix elements Γ^{02}_{01} and $\Gamma^{02}_{02}-\frac{3}{2}\Gamma^{02}_{00}$).[11,24]

In Eq. (24), the term in brackets does not exist for ADDS measurements. The equation thus reduces to

$$I_{\mathrm{ADDS}}(v)\propto\frac{1}{4}\left[\left[\frac{d\sigma}{d\Omega}\right]_{1/2}+3\left[\frac{d\sigma}{d\Omega}\right]_{3/2}\right]+\tfrac{3}{4}\cos^2\beta\left[\left[\frac{d\sigma}{d\Omega}\right]_{1/2}-\left[\frac{d\sigma}{d\Omega}\right]_{3/2}\right]. \quad (25)$$

Equation (25) allows one to determine the variation of the ADDS signal as the polarization angle β of the pump laser is varied in an experiment where the probe laser frequency is set at a fixed value. This variation has been simulated for process (2) under realistic experimental conditions using the theoretical results of Sec. V and the averaging procedure of Sec. II C. The corresponding results are shown in Fig. 9 for various values of the probe laser frequency, i.e., at various scattering angles of the $\mathrm{K}(4P_{1/2})$ atoms. A qualitative difference is observed with what is seen above in conventional differential cross-section measurements. The extrema of I_{ADDS} are found for $\beta=0°$ or 90° without shifts.

When $\beta=0$, the colliding system is entering the $B\,\Sigma_{1/2}$ potential curve. For large values of v, i.e., in the region of backward scattering, the results of Fig. 9 show that this approach favors process (2). In the region of forward scattering, i.e., for small values of v, the reverse is observed. These predictions are easy to rationalize if we remember that collisions at small impact parameters appear in the backward scattering region, and that collisions at large impact parameters are seen in the forward region. Following the analysis of Ref. 11 we can state that at small impact parameters, atoms prepared asymptotically to enter the collision on the $B\,\Sigma_{1/2}$ curve tends to keep this symmetry until the region of $B\,\Sigma_{1/2}$-$A\,\Pi_{1/2}$ radial coupling is reached. We recall that this coupling as well as the $A\,\Pi_{3/2}$-$A\,\Pi_{1/2}$ rotational coupling are well known to be responsible for FST process. On the contrary, for large impact parameters, only an asymptotic preparation on the $A\,\Pi_{3/2}$ curve allows the system to reach the region of radial coupling in approximate $B\,\Sigma_{1/2}$ symmetry. On this basis, the features of Fig. 9 illustrate that the main mechanism responsible for process (2) is the above cited radial coupling: for small impact parameters this coupling is the only one to play a major role, and at large impact parameters, it is preceded by a rotational coupling $A\,\Pi_{3/2}$-$B\,\Sigma_{1/2}$. Such a behavior has already been discussed when considering the total cross section for process (3).[4]

The example of Fig. 9 shows how polarization effects can be used in ADDS measurements to obtain information on the collision dynamics. Using the excitation scheme of Fig. 8 and looking to the position of the maxima and minima of the ADDS signal as β is varied, it is possible to know which alignment of the excited atomic orbital is favorable to induce the inelastic process under study.

Other excitation schemes than that of Fig. 8 are also possible. Because of the cylindrical symmetry in ADDS measurements, these excitation schemes do not lead to information other than that obtained with the scheme of Fig. 8. In this respect, the present section can be considered as providing a general discussion of polarization effects under ADDS measurements.

VIII. CONCLUSION

Differential cross sections of fine-structure transitions in the $4\,^2P$ level of K induced by low-energy collisions with He and Ar have been determined both experimentally and theoretically. The experiment has been performed in a cross-beam apparatus, using the ADDS technique (angular distribution using the Doppler shift). This has made possible a direct comparison in the center-of-mass reference frame between experimental data and quantum-mechanical calculations performed with various sets of interaction potentials. Special care has been taken in this study to polarization effects which are due to the polarization of the K atoms before the collision and the angular resolution of the experimental method which is taken into account by an appropriate numerical averaging of the theoretical predictions.

This work has allowed a sensitive test of the various potential sets available for the K-He and K-Ar systems. The most interesting result concerns the l-dependent pseudopotential set describing the K-He interaction. At present this potential allows one to interpret all the available experimental data concerning the FST process $\mathrm{K}(4P_{3/2}\leftrightarrow 4P_{1/2})$-He: differential cross section, polarization effects, absolute value, and energy dependence of the total cross section. This situation has been encountered without fitting any parameters of the potential set to experimental data. This illustrates that the l-dependent pseudopotential method is a powerful tool for predicting alkali-metal—rare-gas interaction potentials.

When considering the $\mathrm{K}(4P)$-Ar system, none of the available potential sets are found accurate enough to account for the differential cross-section measurements performed in the present study, even those which were found realistic for interpreting total cross-section experimental data. This suggests the need for improvements in the theoretical methods used to calculate K-Ar interaction potentials.

The final aspect of this work concerns polarization effects in ADDS measurements. A general formulation has been given and a "real size" theoretical simulation has been performed taking the $\mathrm{K}(4P_{3/2}\rightarrow 4P_{1/2})+\mathrm{He}$ collision as an example. It has been possible to determine which excitation scheme of the $4P_{3/2}$ level must be used

to get information on the collision dynamics and what kind of information can be actually obtained. The conclusion drawn from this particular example are easy to generalize to other collisional processes where electronic excitation is involved in both the entrance and the exit channels.

ACKNOWLEDGMENTS

The authors wish to thank A. Binet and P. Meynadier for their contribution to the experimental part of this work. They also acknowledge J. R. Manson and R. E. Olson for a careful reading of the manuscript.

APPENDIX

The collision matrix Γ is given by

$$\langle 1/2\, m_{1/2} \mid \Gamma(4P_{3/2}\ \mathbf{k}_{3/2} \rightarrow 4P_{1/2}\ \mathbf{k}_{1/2}) \mid 3/2\, m_{3/2} \rangle = \frac{2i\pi}{\sqrt{k_{3/2}k_{1/2}}} \sum_{l,m_l} \sum_{l',m_{l'}} i^{l-l'} Y^*_{l m_l}(\hat{\mathbf{k}}_{1/2}) Y_{l' m_{l'}}(\hat{\mathbf{k}}_{3/2}) T(3/2\, m_{3/2}\, l'\, m_{l'}; 1/2\, m_{1/2}\, l\, m_l) \ , \quad \text{(A1)}$$

where T is the T matrix associated with the collisional process under study, and Y_{lm_l} are spherical harmonics. The matrix Γ has the following general properties:[3]

$$\langle 1/2\, m_{1/2} \mid \Gamma(4P_{3/2}\, \mathbf{k}_{3/2} \rightarrow 4P_{1/2}\, \mathbf{k}_{1/2}) \mid 3/2\, m_{3/2} \rangle = \langle 1/2\, m_{1/2} \mid \Gamma(4P_{3/2}\, -\mathbf{k}_{3/2} \rightarrow 4P_{1/2}\, -\mathbf{k}_{1/2}) \mid 3/2\, m_{3/2} \rangle \ ,$$

$$\langle 1/2\, m_{1/2} \mid \Gamma(4P_{3/2}\, \mathbf{k}_{3/2} \rightarrow 4P_{1/2}\, \mathbf{k}_{1/2}) \mid 3/2\, m_{3/2} \rangle = (-1)^{1/2+m_{1/2}} (-1)^{3/2+m_{3/2}} \langle 1/2\, -m_{1/2} \mid \Gamma(4P_{3/2}\, \mathbf{k}_{3/2} \rightarrow 4P_{1/2}\, \mathbf{k}_{1/2}) \mid 3/2\, -m_{3/2} \rangle \ , \quad \text{(A2)}$$

$$\langle 1/2\, m_{1/2} \mid \Gamma(4P_{3/2}\, \mathbf{k}_{3/2} \rightarrow 4P_{1/2}\, \mathbf{k}_{1/2}) \mid 3/2\, m_{3/2} \rangle = -\langle 3/2\, m_{3/2} \mid \Gamma(4P_{1/2}\, \mathbf{k}_{1/2} \rightarrow 4P_{3/2}\, \mathbf{k}_{3/2}) \mid 1/2\, m_{1/2} \rangle^* \ .$$

The irreducible components $\Gamma^{k'k}_{q'q}$ of the generalized collision matrix are given by

$$\Gamma^{k'k}_{q'q} = \sum_{\substack{m_{3/2}, m'_{3/2} \\ m_{1/2}, m'_{1/2}}} (-1)^{3/2-m_{3/2}} (-1)^{1/2-m_{1/2}} (2k+1)^{1/2} (2k'+1)^{1/2} \times \begin{pmatrix} \frac{3}{2} & \frac{3}{2} & k \\ m_{3/2} & -m'_{3/2} & -q \end{pmatrix} \begin{pmatrix} \frac{1}{2} & \frac{1}{2} & k' \\ m_{1/2} & -m'_{1/2} & -q' \end{pmatrix}$$

$$\times \langle 1/2\, m_{1/2} \mid \Gamma \mid 3/2\, m'_{3/2} \rangle \langle 3/2\, m_{3/2} \mid \Gamma \mid^{\dagger} \mid 1/2\, m'_{1/2} \rangle \ . \quad \text{(A3)}$$

When Eq. (A2) is inserted into (A3), the following general properties of the $\Gamma^{k'k}_{q'q}$'s are obtained:

$$\Gamma^{k'k}_{q'q} = (-1)^{k'+k} (\Gamma^{k'k}_{q',q})^* \ ,$$

$$\Gamma^{k'k}_{q'q} = (-1)^{q'+q} (\Gamma^{k'k}_{-q'-q})^* \ , \quad \text{(A4)}$$

$$\Gamma^{k'k}_{00} \neq 0 \ \text{ only if } k+k' \text{ even} \ ,$$

$\Gamma^{k'k}_{q'q}$ is real if $k+k'$ is even and pure complex is even if $k+k'$ odd.

If the collisional problem under study has specific symmetries, additional properties are found for $\Gamma^{k'k}_{q'q}$.

(i) If the collision has cylindrical symmetry with respect to the quantization axis [i.e., if in Eq. (A1) integration is performed over the azimuthal angle of the wave vector $\mathbf{k}_{1/2}$ of the scattered atoms] then

$$\Gamma^{k'k}_{q'q} = \delta_{q'q} \Gamma^{k'k}_{qq} \ . \quad \text{(A5)}$$

(ii) If the collision has a spherical symmetry [i.e., if integration is performed in Eq. (A1) over both polar and azimuthal angles of $\mathbf{k}_{1/2}$] then

$$\Gamma^{k'k}_{q'q} = \delta_{q'q} \delta_{k'k} \Gamma^{kk}_{qq} \ . \quad \text{(A6)}$$

[1] E. E. Nikitin, Adv. Chem. Phys. **28**, 317 (1975).
[2] R. H. G. Reid, J. Phys. B **6**, 2018 (1973).
[3] F. H. Mies, Phys. Rev. A **7**, 942 (1973).
[4] J. Pascale, J. M. Mestdagh, J. Cuvellier, and P. de Pujo, J. Phys. B **17**, 2627 (1984).
[5] J. Pascale, Phys. Rev. A **28**, 632 (1983).
[6] J. Pascale, in *Proceedings of the XIIIth Summer School on Quantum Optics,* edited by J. Fiutak and J. Mizerski (World Scientific, Singapore, 1986), p. 38–93.
[7] A. Chebanier de Guerra and F. Masnou-Seeuw, in *Preparation and Proceedings of the 13th International Conference on Physics of Electronic and Atomic Collisions, Berlin,* edited by J.

Eichler *et al.* (North-Holland, Amsterdam, 1983), Abstract, p. 314. The core-core interaction $K^{\dagger}$-Ar of N. A. Sondergaard and E. A. Mason [J. Chem. Phys. **62**, 1299 (1975)] are used to define these potentials. This point is discussed in Ref. 4.

[8]R. Düren, E. Hasselbrink, and G. Moritz, Z. Phys. A **307**, 1 (1982).

[9]J. Pascale and J. Vandeplanque, J. Chem. Phys. **60**, 2278 (1974).

[10]J. M. Mestdagh, J. Berlande, P. de Pujo, J. Cuvellier, and A. Binet, Z. Phys. A **304**, 3 (1982).

[11]I. V. Hertel, H. Schmidt, A. Bahring, and E. Meyer, Rep. Prog. Phys. **48**, 375 (1985).

[12]J. Pascale and M. Y. Perrin, J. Phys. B **13**, 1839 (1980).

[13]J. L. Kinsey, J. Chem. Phys. **66**, 2560 (1977).

[14]W. D. Phillips, J. A. Serri, D. J. Ely, D. E. Pritchard, K. R Way, and J. L. Kinsey, Phys. Rev. Lett. **41**, 937 (1978).

[15]J. A. Serri, J. L. Kinsey, and D. E. Pritchard, J. Chem. Phys. **75**, 663 (1981).

[16]R. Düren, E. Hasselbrink, and G. Hillrichs, Chem. Phys. Lett. **112**, 441 (1984).

[17]J. Cuvellier, J. M. Mestdagh, J. Berlande, P. de Pujo, and A. Binet, Rev. Phys. Appl. **16**, 679 (1981),

[18]A. Omont, Prog. Quantum Electron. **5**, 69 (1977).

[19]R. P. Saxon, R. E. Olson, and B. Liu, J. Chem. Phys. **67**, 2692 (1977).

[20]R. H. G. Reid, J. Phys. B **8**, L493 (1975).

[21]F. Masnou-Seeuws, M. Philippe, E. Roueff, and A. Spielfiedel, J. Phys. B **12**, 4065 (1979).

[22]R. Olson and F. Smith, Phys. Rev. A **3**, 1607 (1971).

[23]R. Düren, E. Hasselbrink, and G. Hillrichs, in *Verhandlungen der Deutsche Physikalische Gesellschaft, Heidelberg, 1986,* (Physik-Verlag, Weinheim, West Germany, 1986), Vol. 21.

[24]I. V. Hertel and H. Schmidt, Comments At. Mol. Phys. (to be published).